Engineered Science
DOI: https://dx.doi.org/10.30919/es1390

Application of Genetic Algorithms in the Design of Hybrid Fractal Microstrip Antennas Based on Minkowski and Sierpinski Carpet Patterns

Chanchai Thaijiam*

Abstract

With wireless multifrequency applications, this research paper presents how to use genetic algorithms (GA) to design a hybrid fractal microstrip antenna based on the Minkowski and Sierpinski carpet fractal microstrip structures. The traditional design of fractal antennas uses the iterated function system (IFS), which has difficulty in finding flexible dimensional scales to match every desired operating frequency. GA can generate dimensional scales flexibly with constraints to control desired antenna parameters. This allows for maintaining control over dimensional scales when designing complex antenna shapes. Different shapes of patch antenna are optimized using GA with dynamic changes to the antenna geometry at each desired operating frequency. The optimization and simulation were conducted using the matrix laboratory (MATLAB) programming language and computer simulation technology (CST) microwave studio programs. The desired frequencies operate in the frequency range of 0.7 - 2.6 GHz. The antenna configurations were optimized to achieve resonance and transformation frequencies, and the microstrip feedlines were matched to minimize return losses of less than -15 dB. Both simulated and experimental results for the antenna design are presented. Finally, the crucial requirements of the antenna design and the proposed GA optimization are summarized.

Keywords: Genetic algorithms; Optimized geometric structure; Minkowski pattern; Sierpinski carpet pattern; Hybrid fractal antenna.
Received: 21 November 2023; Revised: 18 December 2024; Accepted: 06 January 2025.
Article type: Research article.

1. Introduction

Wireless multifrequency applications use multifrequency antennas, such as wireless local-area network (WLAN) technology, wireless sensor networking, radio frequency identification (RFID) technology, and cellular telephone service. A popular multifrequency antenna is a fractal microstrip patch antenna, known for its low profile, small size, lightweight, low cost, ease of fabrication, easy integration into circuits, and high efficiency. This type of antenna is designed to achieve a compact and multifrequency patch.

Wireless sensor networks consist of strategically spread antennas, allowing dedicated sensors to monitor and transmit collected data to a central hub. This setup evaluates schemes for energy efficiency, achievable rates, and distributed energy.[1-3] Multifrequency antennas are especially applied to multifrequency media access control for wireless sensor networks. Arbitrary shapes of antenna structures can generate multifrequency radiation; however, asymmetrical geometry may be a concern.[4-6] Minkowski and Sierpenski carpet fractal antennas are multifrequency types, offering a small patch.[7,8] These antennas have been extensively explored in fractal geometry for modern antenna design.[9] A traditional fractal antenna comprises unique geometric shapes with self-similarity, leading to its multifrequency feature. Theoretically, altering the geometric shapes during transformation can impact the frequencies.[10] For instance, reducing the width and length by three times (scaling factor) in each transformation triples the frequencies from the previous shape. Note that the fixed frequencies designed from the traditional fractal antenna transformation iteration method (the iterated function system, IFS) may not align with the practical needs of the fixed scaling factors.[7-8,11] The fixed scaling factors can affect dimensional scales in the inflexible design of antenna structures.

The feedline's placement can impact the reflection coefficient by altering an antenna's input impedance.[12-14] The feedline is designed based on the antenna's impedance to

Department of Electrical Engineering, Faculty of Engineering, Srinakharinwirot University, Ongkharak Campus, Nakhon-Nayok, 26120, Thailand
**Email:* chanchait@g.swu.ac.th (C. Thaijiam)

optimize the antenna's efficiency. When the structure of an antenna is modified, its input impedance also changes. A microstrip feedline can be easily integrated with electronic circuits in microwave wireless devices. However, matching impedances between an antenna and a feedline becomes more difficult if the input impedance of the antenna shifts due to fractal transformation.

The research papers discuss the application of genetic algorithms (GA) for optimizing microstrip patch antennas.[15-17] They highlight the use of GA for binary optimization of microstrip antennas and its effectiveness in generating small rectangular microstrip patches of arbitrary shape. Furthermore, the research paper explores the local optimization of a Sierpinski carpet fractal antenna, resulting in improved resonance and transformation behaviors.[18] However, the research can be improved by using a global optimizer. Nonetheless, geometric overlap poses a challenge to achieving the optimization goal of fractal geometry. The research paper discusses overlap detection,[19] an important aspect of packing and motion-planning problems, and shows the Minkowski fractal difference when done on shapes. Finally, the research papers suggest that combining different geometric shapes can help avoid geometric overlap and increase the chances of selecting more than one geometry to create a fractal antenna.[20,21]

This research paper presents a design for a single-layer microstrip patch antenna. The design incorporates Minkowski and Sierpinski carpet fractal geometries, along with a microstrip transmission feedline for seamless integration into modern electronic circuits. While previous research has examined the configuration of this combined antenna design,[20,21] the optimal selection of resonance and transformation frequencies based on these configurations has not been explored using GA. In addition, this paper focuses on preventing overlap of the geometric antenna structure in the GA constraints for designing the antenna. This study aims to enhance the performance of antenna designs for the multifrequency range. The study proposes a new hybrid fractal microstrip antenna design that combines the Minkowski and Sierpinski carpet structures. This design uses genetic algorithms to achieve the desired operating frequencies, unlike the typical design approach that employs integrated frequency synthesis.[7-8,13-14,20,21]

This paper is structured as follows. Section 2 outlines the methodology, which describes antenna configurations, design procedures, and experiments. This section explains how to optimize the antenna configurations using GA to meet design objectives and how to conduct an experiment. Section 3 presents the results, and Section 4 is the discussion. Finally, Section 5 contains the conclusion.

2. Methodology

2.1 Proposed fractal microstrip antenna

A microstrip patch antenna can be constructed using a printed circuit board (PCB) with two conductive layers of annealed copper laminated on both faces of a dielectric layer. The patch features are etched on one side while the other serves as a ground plane.

$$W_0 = \frac{c}{2f_0}\sqrt{\frac{2}{\varepsilon_r+1}} \quad (1)$$

$$L_0 = L_{eff} - 2\Delta L \quad (2)$$

$$L_{eff} = \frac{c}{2f_0\sqrt{\varepsilon_{reff}}} \quad (3)$$

$$\Delta L = 0.412h\frac{(\varepsilon_{reff}+0.3)\left(\frac{W_0}{h}+0.264\right)}{(\varepsilon_{reff}+0.258)\left(\frac{W_0}{h}+0.8\right)} \quad (4)$$

$$\varepsilon_{reff} = \frac{\varepsilon_r+1}{2} + \frac{\varepsilon_r-1}{2}\left(1+12\frac{h}{W_0}\right)^{-\frac{1}{2}} \quad (5)$$

A rectangular microstrip patch antenna with a microstrip feedline is shown in Fig. 1(a), and the transmission line and cavity models are used to analyze the antenna.[22] A rectangular microstrip patch antenna is calculated from Eqs. (1)-(5). The physical width (W_0) and length (L_0) of a rectangular microstrip patch antenna are shown in Eqs. (1) and (2), respectively. At the desired operating frequency (f_0), a dielectric layer's relative permittivity (ε_r) is related to the antenna design. c is the velocity of light in free space. Because of the fringing effects, the effective length (L_{eff}) in Eq. (3) is greater than the physical length (L_0) in Eq. (2) with an extension on each end by a distance (ΔL) in Eq. (4). $\frac{W_0}{h}$ is the width-to-height ratio where h is the dielectric layer height or substrate thickness. ε_{reff} is the effective dielectric constant, as shown in Eq. (5). Note that the international system (SI) of units is used in Eqs. (1)-(5). Figs. 1(b) and (c) show the first iteration of the Minkowski fractal microstrip antenna and a hybrid (combined) Minkowski and Sierpinski carpet fractal microstrip antenna, respectively. The geometric shapes of fractal antennas are typically transformed relative to a constant ratio of cutting slots in dimensions,[23,24] resulting in transformation frequencies with this ratio (the scaling factor). This research paper employs GA to design the antennas due to the difficulty of manually finding the perfect scaling factor match for every desired operating frequency with the typical design approach that uses IFS.[7,8]

2.2 Design procedure with GA

Fig. 1 illustrates the antenna configuration stage of the n^{th} iteration. Initially, the physical width and length of a rectangular patch (the zero iteration) are W_0 and L_0, respectively. For a rectangular microstrip patch antenna, the dimensions W_0 and L_0 are usually unequal in the dominant mode.[22] However, artificial intelligence is required to design a customized arbitrarily shaped microstrip patch antenna, such as a hybrid fractal microstrip antenna based on Minkowski and

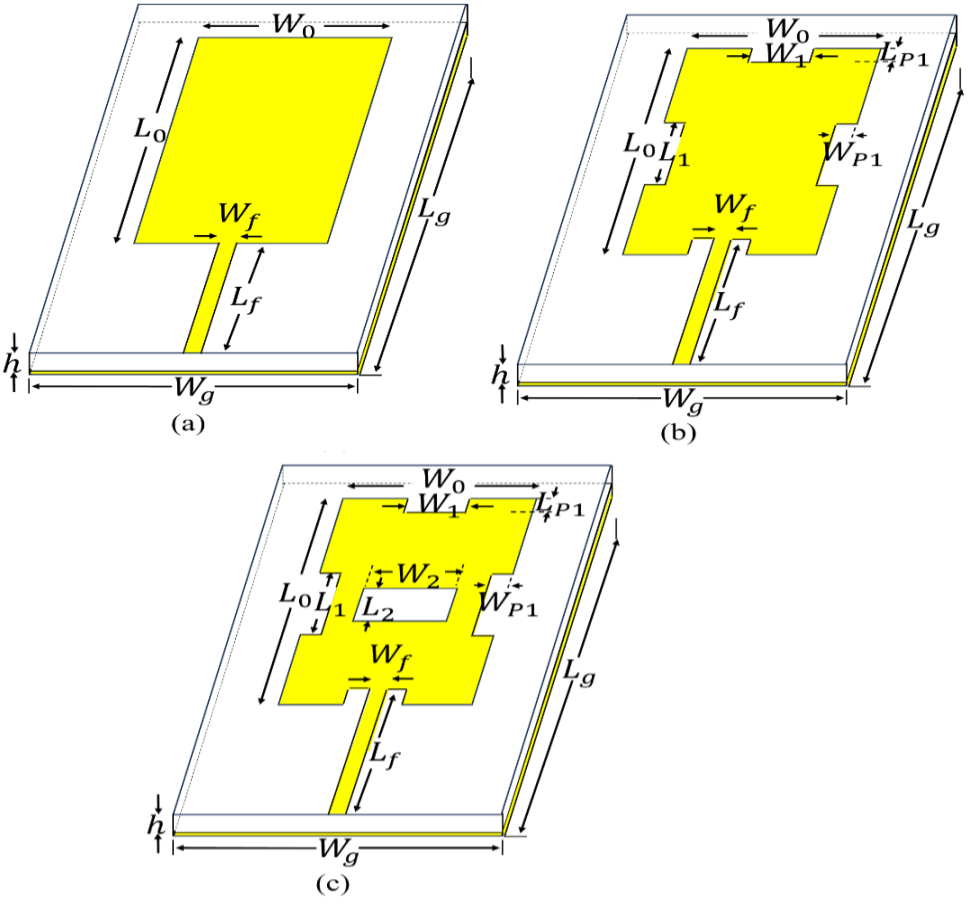

Fig. 1: Configurations of microstrip patch antennas are as follows: (a) a rectangular patch (the zero iteration), (b) the first iteration of the Minkowski fractal, and (c) the hybrid Minkowski and Sierpinski carpet fractal.

Sierpinski carpet structures. The cutting slots on a microstrip patch antenna can be flexibly sized to accommodate the arbitrarily geometric shapes of the fractal antenna design. The following text contains the GA optimization method for configuring the antenna structure during each iteration of the Minkowski fractal microstrip antenna and the Sierpinski carpet fractal microstrip antenna.[23,24] However, they do not explain using GA to optimize a hybrid fractal microstrip antenna that combines Minkowski and Sierpinski carpet structures. Changing the scaling factor's ratios during each iteration can alter the desired operating frequencies. GA is used to design antennas for the desired operating frequencies while ensuring that the antenna configurations do not overlap geometrically. GA can be used to approach the desired operating frequencies and design the antenna configurations.

GA optimizes the antenna configurations at desired resonance and transformation frequencies.[25,26] The antennas are simulated by programming computer simulation technology (CST) programs and MATLAB programming language codes.[27,28] Fig. 2 illustrates the process of designing the antenna structure with resonance and transformation frequencies using GA optimization. To generate a rectangular patch, W_0 and L_0 (see Fig. 1(a)) of a rectangular microstrip patch antenna are set as GA parameters. Next, the first iteration of the Minkowski fractal microstrip patch antenna is designed for W_0, L_0, W_1, L_{P1}, W_{P1}, and L_1 as GA parameters to generate a rectangular patch and cutting slots (see Fig. 1(b)). Then, W_0, L_0, W_1, L_{P1}, W_{P1}, L_1, W_2, and L_2 are set as GA parameters to design the hybrid Minkowski and Sierpinski carpet fractal microstrip antenna (see Fig. 1(c)). Lastly, W_f and L_f are also set as GA parameters that are considered for matching purposes of a feedline. Please note that W_g and L_g of a ground plane are set to be double the patch size. A dielectric or substrate layer's relative permittivity (ε_r) and a dielectric layer height or substrate thickness (h) are constant values known from the characteristics of a printed circuit board (PCB) and used to construct the microstrip antenna. The dimensions of microstrip patch antennas and feedlines are randomly generated as initial populations. Please note that the initial widths and lengths of the antenna configurations are set as GA parameters from calculating by Eqs. (1)-(5). These dimensions are generated with the constraint of avoiding geometric overlap in the antenna configurations using GA MATLAB code. Each configuration is then modeled in CST,

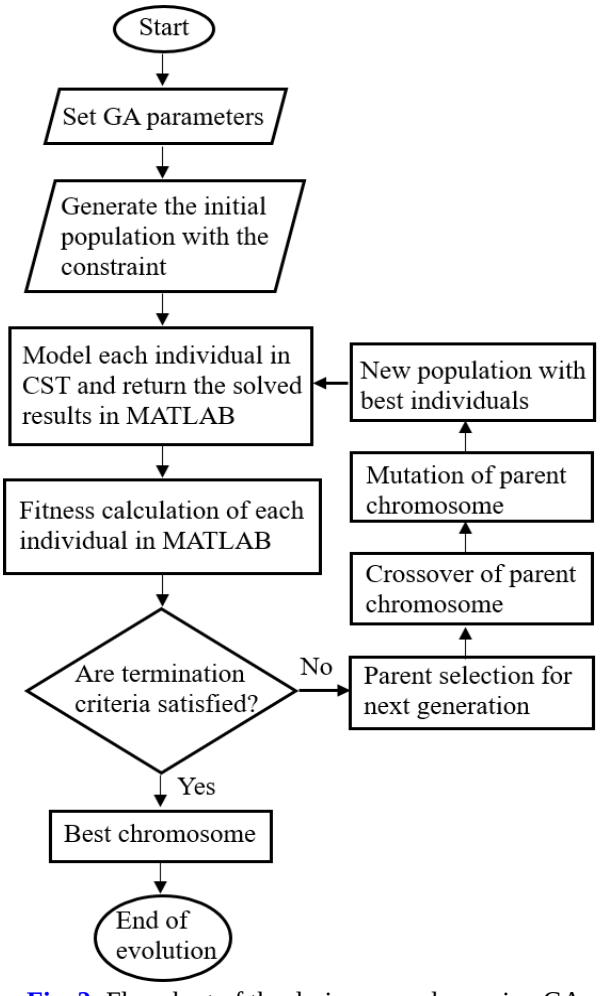

Fig. 2: Flowchart of the design procedure using GA.

which returns resonance and transformation frequencies as well as $S11$ parameters (as shown in Fig. 3). The $S11(f_n)$ parameters are dependent on both resonance and transformation frequencies.

$$Fitness\ function = \frac{1}{N+1}\sum_{n=0}^{N} S11(f_n) \quad (6)$$

where $S11(f_n) = S11(f_n)$ in case of $S11(f_n) \geq$ -15 dB, and $S11(f_n) =$ -15 in case of $S11(f_n) <$ -15 dB ($n = 0$ for resonance frequency, and $n = 1$ to N for transformation frequencies). The fitness function of Eq. (6) is minimized to -15 dB for GA. The frequencies (f_n) can be resonance and transformation frequencies: the resonance frequency (f_0) for a rectangular microstrip patch antenna, the first transformation frequency (f_1) for the Minkowski fractal structure, and the second transformation frequency (f_2) for the hybrid fractal microstrip antenna based on Minkowski and Sierpinski carpet structures.

If the termination criteria of GA, relative to Eq. (6), are fulfilled, then the optimized widths and lengths of the microstrip patch antenna, along with the optimized width and length of the feedline, represent the best chromosomes to achieve the desired operating frequencies and $S11$ parameters. Conversely, if the termination criteria for the GA are not met, the GA process will proceed to the next generation. This

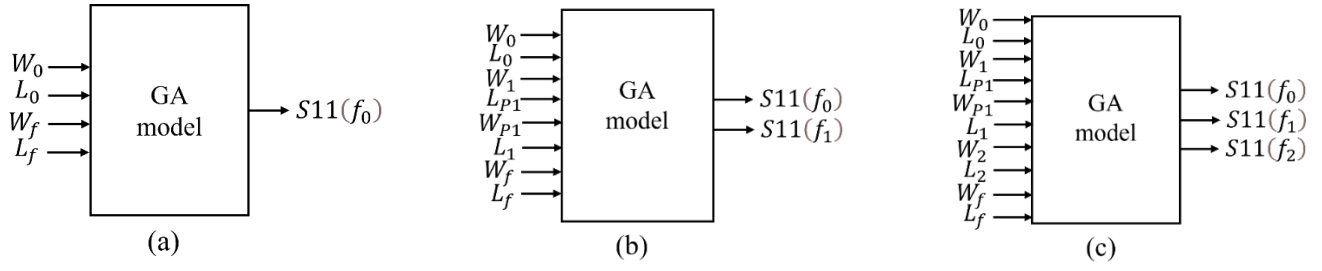

Fig. 3: Proposed GA models: (a) for a rectangular microstrip patch antenna, (b) for the first transformed Minkowski fractal microstrip patch antenna, and (c) for the hybrid fractal microstrip patch antenna based on Minkowski and Sierpinski carpet structures.

Table 1: Geometric dimensions of the microstrip patch antennas at 0.7, 1.8, and 2.6 GHz.

Microstrip patch antennas	W_0	L_0	W_1	L_{P1}	W_{P1}	L_1	W_2	L_2	W_f	L_f
The rectangular microstrip	124.92	98.22	-	-	-	-	-	-	1.75	71.53
The first iteration of the Minkowski fractal microstrip	133.50	98.98	72.93	2.47	5.58	68.10	-	-	3.55	83.33
The hybrid Minkowski and Sierpinski carpet fractal microstrip	133.36	102.75	73.96	4.51	2.97	71.02	11.36	3.68	6.07	88.50

Note that geometric dimensions are in millimeter (mm) units. The substrate material is FR4, and the substrate thickness (h) is 1.6 mm. W_g and L_g of the ground plane are -W_0 to W_0 and $-0.5L_0 - L_f$ (for the rectangular microstrip), $-0.5L_0 -(L_f - L_{P1})$ (for the first iteration of the Minkowski fractal microstrip and the hybrid Minkowski and Sierpinski carpet fractal microstrip) to L_0 mm, respectively.

involves selecting parent chromosomes, performing crossover between them, mutating the parent chromosomes, and creating a new population. This new population will consist of the best individuals, which include the updated widths and lengths of the microstrip patch antennas and the feedlines. The crucial requirements and the proposed GA optimization of the antenna design are compared with experimental results.

2.3 Experiment

The electronic network analyzer (ENA) series vector network analyzer manufactured by Agilent Technologies, along with the two-part test set, is used to measure all S-parameters and far-field antenna patterns within a frequency range of 100 kHz to 4.5 GHz. The calibration process is carefully managed to ensure consistency in measurement standards. Compared to the CST simulation results, the antenna is rotated in an anticlockwise direction at five-degree increments to cover 360 degrees. The proposed fractal microstrip antennas are milled on the copper side of the FR-4 substrate using the LPKF-42 Protomat milling machine. The radiation patterns are measured in an anechoic chamber at Srinakharinwirot University (see Fig. 4).

3. Results

The dimensions of the rectangular microstrip patch antenna at 0.7 GHz, the first iteration of the Minkowski fractal microstrip patch antenna at 0.7 and 1.8 GHz, and the hybrid Minkowski and Sierpinski carpet fractal microstrip patch antenna at 0.7, 1.8, and 2.6 GHz for optimal design by GA are all listed in Table 1. The optimization of the widths and lengths of the feedlines is carried out using the GA techniques. The ground planes' widths and lengths are set to be at least double the widths and lengths of the patch sizes.

The fitness value of GA optimization is shown in Eq. (6) when compared with the generation. When the generations increase, the best fitness and the mean fitness values converge on the same value. The population size based on GA is an important parameter that directly influences the ability to search for an optimum solution. At the 0.7 GHz operating frequency of the rectangular microstrip patch antenna, the feedline's width (W_0), length (L_0), width (W_f), and length (L_f) are set to 124.92, 98.22, 1.75, and 71.53 mm, respectively. For the Minkowski fractal microstrip patch antenna at the 0.7 and 1.8 GHz operating frequencies, the widths (W_0, W_1, and W_{P1}) and lengths (L_0, L_{P1}, and L_1) are 133.50, 72.93, 5.58, 98.98, 2.47, and 68.10 mm, respectively. The width (W_f) and length (L_f) for the microstrip feedline are 3.55 and 83.33 mm, respectively. For the hybrid Minkowski and Sierpinski carpet fractal microstrip patch antenna at 0.7, 1.8, and 2.6 GHz operating frequencies, the widths (W_0, W_1, W_{P1}, and W_2) and lengths (L_0, L_{P1}, L_1, and L_2) are 133.36, 73.96, 2.97, 11.36, 102.75, 4.51, 71.02, and 3.68 mm, respectively, while the width (W_f) and length (L_f) of the microstrip feedline are 6.07 and 88.50 mm, respectively. The optimal sizes of the desired antennas and feedlines are suitable for real-world construction, as indicated in Table 1.

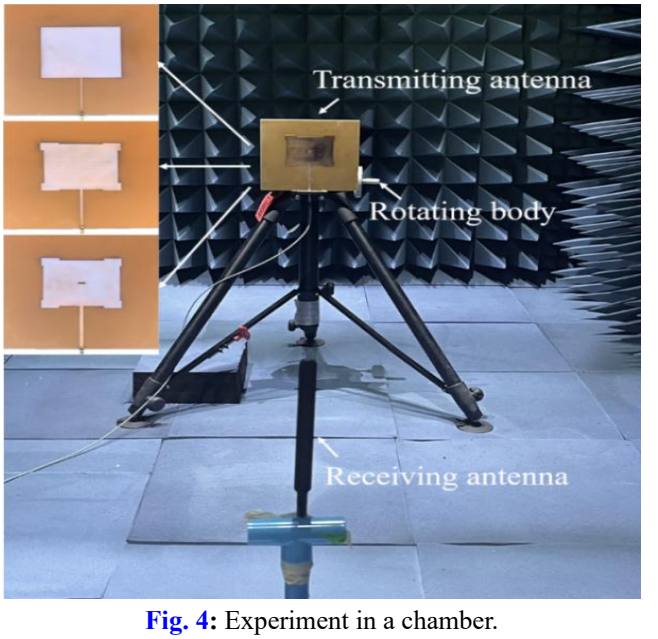

Fig. 4: Experiment in a chamber.

As the generations progress, the best fitness and mean fitness values converge on the same value as shown in Fig. 5. For The first iteration of the Minkowski fractal microstrip

patch antenna, the maximum generation is 25. The population size is an important parameter that directly influences the ability to search for an optimum solution, with a population size of 150. Population size and maximum generation may vary depending on the antenna structure. However, for the evolutionary strategies controller, the graph of fitness values versus the number of successful generations resembles the graph shown in Fig. 5.

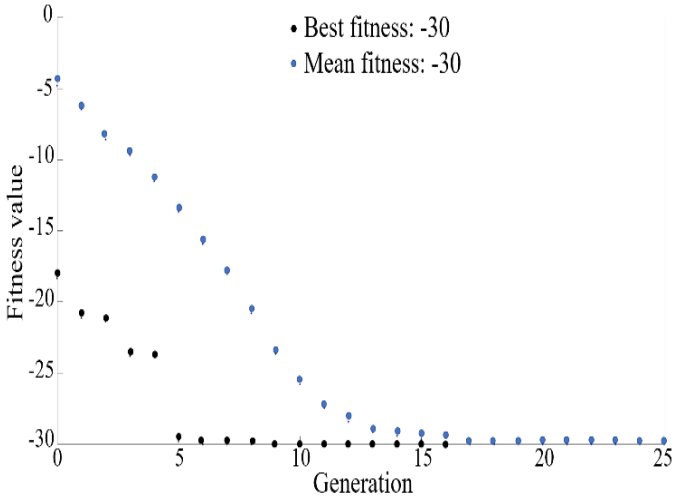

Fig. 5: An example of the fitness values versus the generations of GA optimization.

Fig. 6 displays the microstrip patch antennas that are used to take measurements. The inner conductor pin of the 50 Ω SMA male connector is connected to the microstrip feedline while the outer housing of the same connector is connected to the ground plane of the microstrip antennas. The simulation of the surface current distribution on the microstrip patch antennas is displayed in Fig. 7, as modeled by CST. Please note that the maximum amplitude of the surface current distribution is normalized to 0 dB. This means that the maximum amplitude of the surface current distribution is divided by itself, resulting in a value of 1. Then, the logarithm of 1 is taken, which equals 0 dB.

Figs. 8 and 9 display the $S11$ parameters and 2D far-field patterns of various microstrip patch antennas, respectively. Specifically, these include the rectangular microstrip patch antenna at 0.7 GHz, the first iteration of the Minkowski fractal microstrip patch antenna at 0.7 and 1.8 GHz, and the hybrid Minkowski and Sierpinski carpet fractal microstrip patch antenna at 0.7, 1.8, and 2.6 GHz. The directional gains are compared to the isotropic antenna. Electric and magnetic fields are displayed in an anticlockwise direction, covering 360 degrees. The results from both simulation and experiment are compared to clarify their differences.

Fig. 8 shows the $S11$ parameters on the y-axis, which depend on resonance and transformation frequencies on the x-axis. In Fig. 8(a), for the rectangular microstrip patch antenna, the $S11$ simulation result is -18.16 dB at 0.70 GHz, and the $S11$ measurement result is -15.49 dB at 0.71 GHz. In Fig. 8(b), for the first iteration of the Minkowski fractal microstrip patch antenna, the $S11$ simulation results are -22.72 dB at 0.70 GHz and -25.42 dB at 1.80 GHz, and the $S11$ measurement results are -21.59 dB at 0.71 GHz and -17.07 dB at 1.82 GHz. In Fig. 8(c), for the hybrid Minkowski and Sierpinski carpet fractal microstrip patch antenna, the $S11$ simulation results are -16.57 dB at 0.70 GHz, -20.66 dB at 1.80 GHz, and -18.31 dB at 2.60 GHz, and the $S11$ measurement results are -18.71 dB at 0.71 GHz, -16.99 dB at 1.82 GHz, and -13.99 dB at 2.65 GHz. The graphs also display the fractional matching bandwidths ($S11$ = -10 dB definition). As shown in Fig. 8(a), the rectangular microstrip patch antenna has simulation and measurement results for bandwidth of 15.50 and 19.00 MHz with operating frequencies of 0.70 and 0.71 GHz, respectively. The first iteration of the Minkowski fractal microstrip patch antenna, illustrated in Fig. 8(b), has simulation results for bandwidth of 16.90 and 35.00 MHz with operating frequencies of 0.70 and 1.80 GHz, respectively. The bandwidth measurement results are 21.50 and 36.60 MHz with

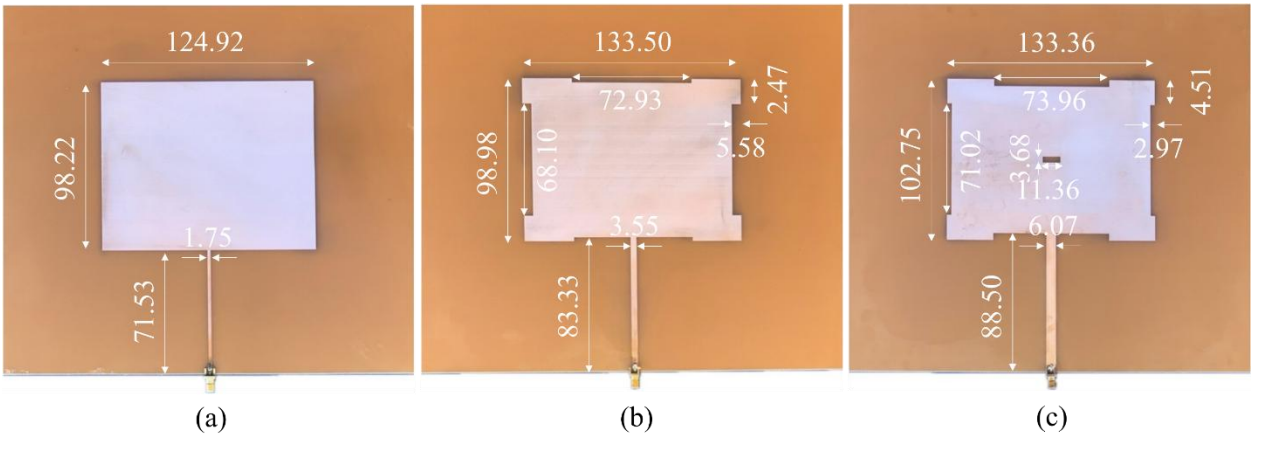

Fig. 6: The desired antenna structures are as follows: (a) the rectangular microstrip patch antenna at 0.7 GHz, (b) the first iteration of the Minkowski fractal microstrip patch antenna at 0.7 and 1.8 GHz, and (c) the hybrid Minkowski and Sierpinski carpet fractal microstrip patch antenna at 0.7, 1.8, and 2.6 GHz.

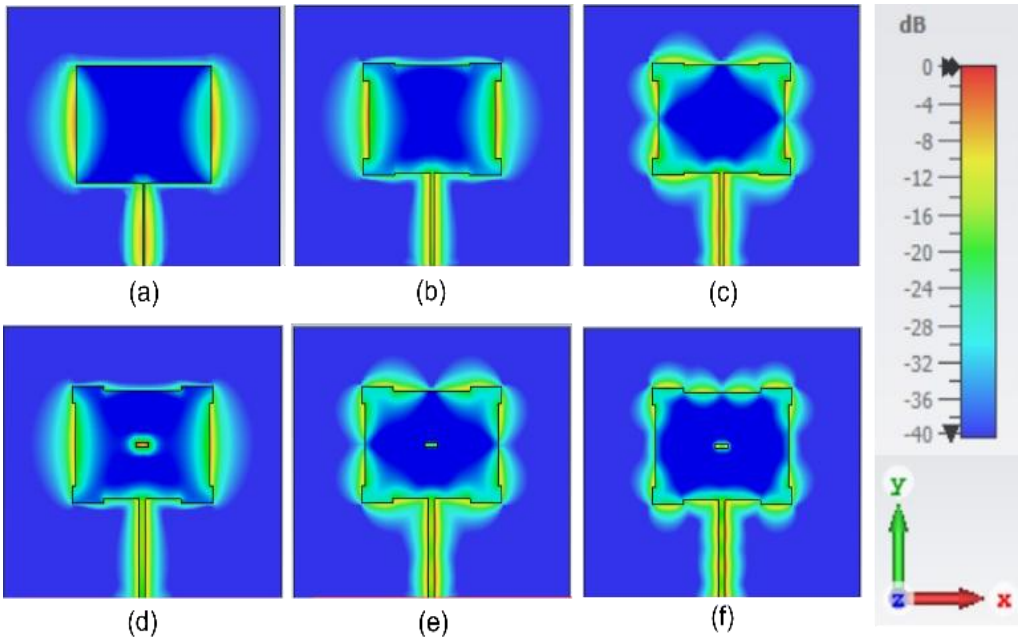

Fig. 7: The surface current distribution on (a) the rectangular microstrip patch antenna at 0.7 GHz, (b) and (c) the first iteration of the Minkowski fractal microstrip patch antenna at 0.7 and 1.8 GHz, respectively, and (d), (e), and (f) the hybrid Minkowski and Sierpinski carpet fractal microstrip patch antenna at 0.7, 1.8, and 2.6 GHz, respectively.

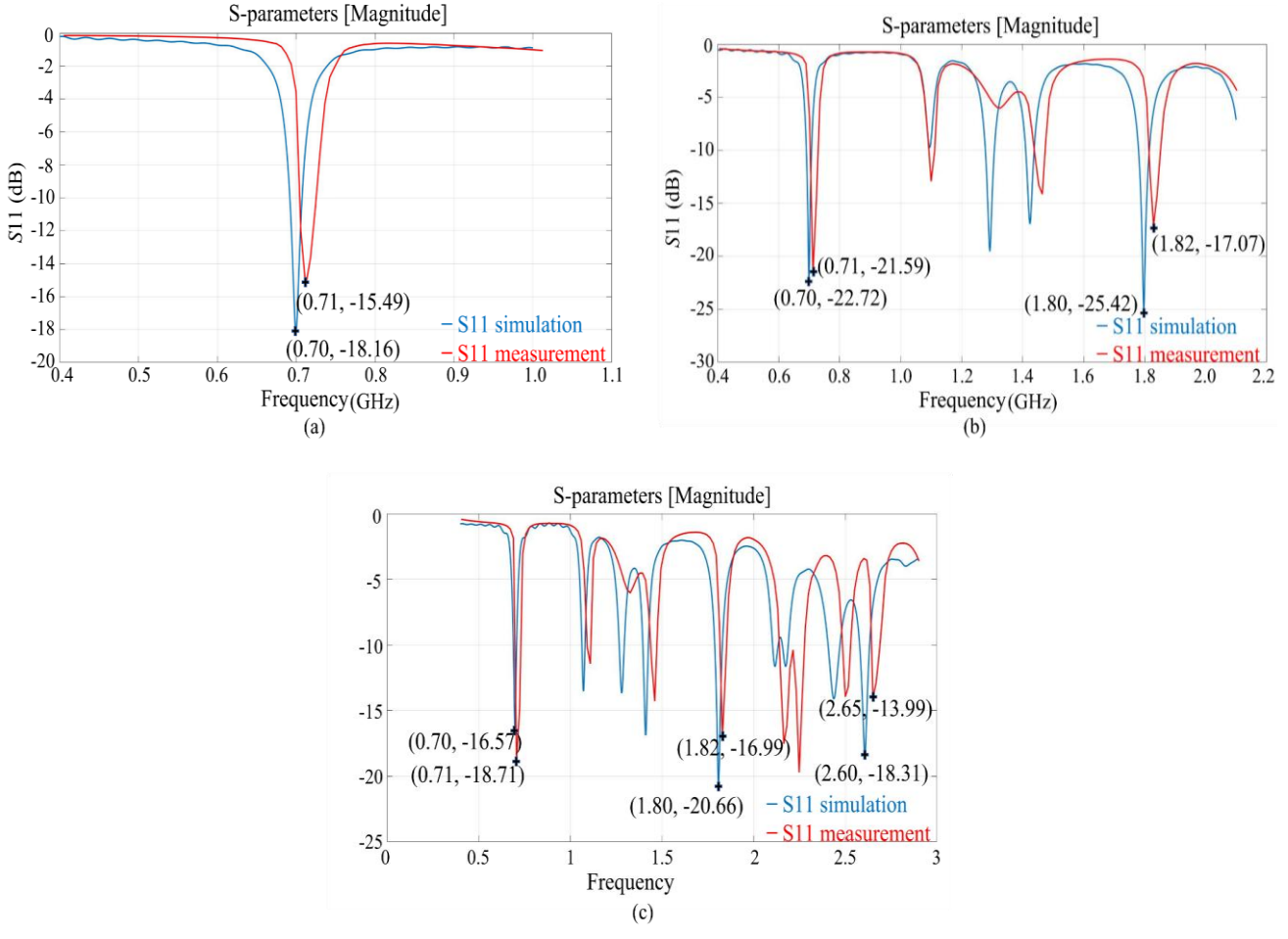

Fig. 8: $S11(f_n)$ parameters depend on resonance and transformation frequencies for (a) the rectangular microstrip patch antenna at 0.7 GHz, (b) the first iteration of the Minkowski fractal microstrip patch antenna at 0.7 and 1.8 GHz, and (c) the hybrid Minkowski and Sierpinski carpet fractal microstrip patch antenna at 0.7, 1.8, and 2.6 GHz. The blue lines represent simulation results, while the red lines depict experimental results.

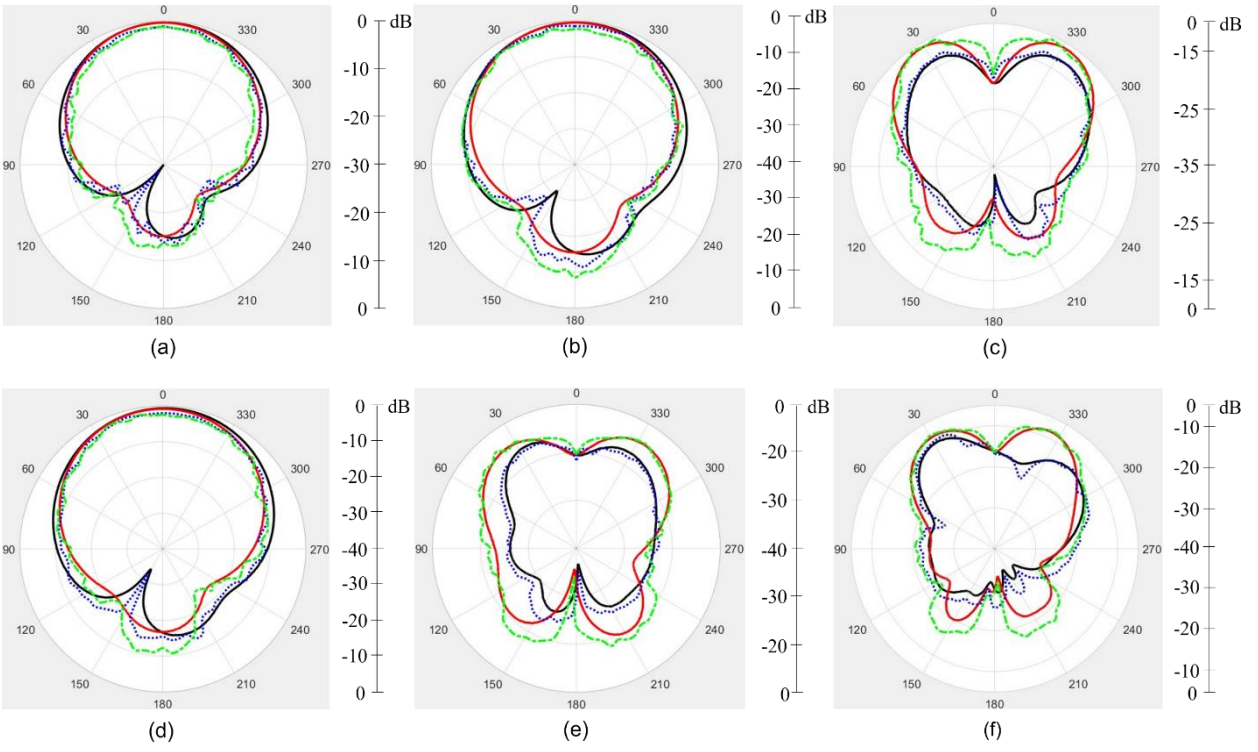

Fig. 9: 2D far-field radiation patterns of the rectangular microstrip patch antenna at 0.70 GHz (a), the first iteration of the Minkowski fractal microstrip patch antenna at 0.70 GHz (b) and 1.80 GHz (c), and the hybrid Minkowski and Sierpinski carpet fractal microstrip patch antenna at 0.70 GHz (d), 1.80 GHz (e), and 2.60 GHz (f). Note that the solid black and red lines show the simulation results of the electric and magnetic fields, respectively. Meanwhile, the dashed blue and green lines show the experiment results of the electric and magnetic fields, respectively.

operating frequencies of 0.71 and 1.82 GHz, respectively. Finally, for the hybrid Minkowski and Sierpinski carpet fractal microstrip patch antenna, depicted in Fig. 8(c), the simulation results for bandwidth are 17.90, 41.60, and 54.10 MHz with operating frequencies of 0.70, 1.80, and 2.60 GHz, respectively. The bandwidth measurement results are 21.50, 40.60, and 50.90 MHz with operating frequencies of 0.71, 1.82, and 2.65 GHz, respectively.

Figs. 9 (a), (b), and (d) show the directions of the electric and magnetic fields' main lobes for different types of microstrip patch antennas operating at a frequency of 0.70 GHz. The rectangular microstrip patch antenna has a main lobe direction of approximately 2.0 degrees with maximum values around 0 dB (simulation results) and -1.07 dB (experiment results) for the electric field and 0.0 degrees with maximum values around 0 dB (simulation results) and -1.23 dB (experiment results) for the magnetic field. The first iteration of the Minkowski fractal microstrip patch antenna has a main lobe direction of approximately 3.0 degrees with maximum values around 0 dB (simulation results) and -0.87 dB (experiment results) for the electric field and 0.0 degrees with maximum values around 0 dB (simulation results) and -2.03 dB (experiment results) for the magnetic field. The hybrid Minkowski and Sierpinski carpet fractal microstrip patch antenna has a main lobe direction of approximately 4.0 degrees with maximum values around 0 dB (simulation results) and -1.96 dB (experiment results) for the electric field and 1.0 degrees with maximum values around 0 dB (simulation results) and -2.04 dB (experiment results) for the magnetic field. In Fig. 9(c), the main lobes' directions of the electric and magnetic fields for the first iteration of the Minkowski fractal microstrip patch antenna at the operating frequency of 1.80 GHz are approximately 34.0 degrees with maximum values around -10.32 dB (simulation results) and -10.46 dB (experiment results) and 32.0 degrees with maximum values around -2.81 dB (simulation results) and -2.87 dB (experiment results), respectively. In Fig. 9(e), the main lobes' directions of the electric and magnetic fields for the hybrid Minkowski and Sierpinski carpet fractal microstrip patch antenna at the operating frequency of 1.80 GHz are approximately 26.0 degrees with maximum values around -14.62 dB (simulation results) and -16.92 dB (experiment results) and 34.0 degrees with maximum values around -8.46 dB (simulation results) and -8.44 dB (experiment results), respectively. Finally, Fig. 9(f) depicts the main lobes' directions of the electric and magnetic fields for the hybrid Minkowski and Sierpinski carpet fractal microstrip patch antenna at the operating frequency of 2.60 GHz, having approximately 28.0 degrees with maximum values around -10.83 dB (simulation results) and -10.76 dB (experiment results) and 26.0 degrees with maximum values around -4.55 dB (simulation results) and -4.56 dB (experiment results), respectively. Please note that the electric and magnetic fields in the far-field region of the microstrip patch antennas are normalized by the maximum

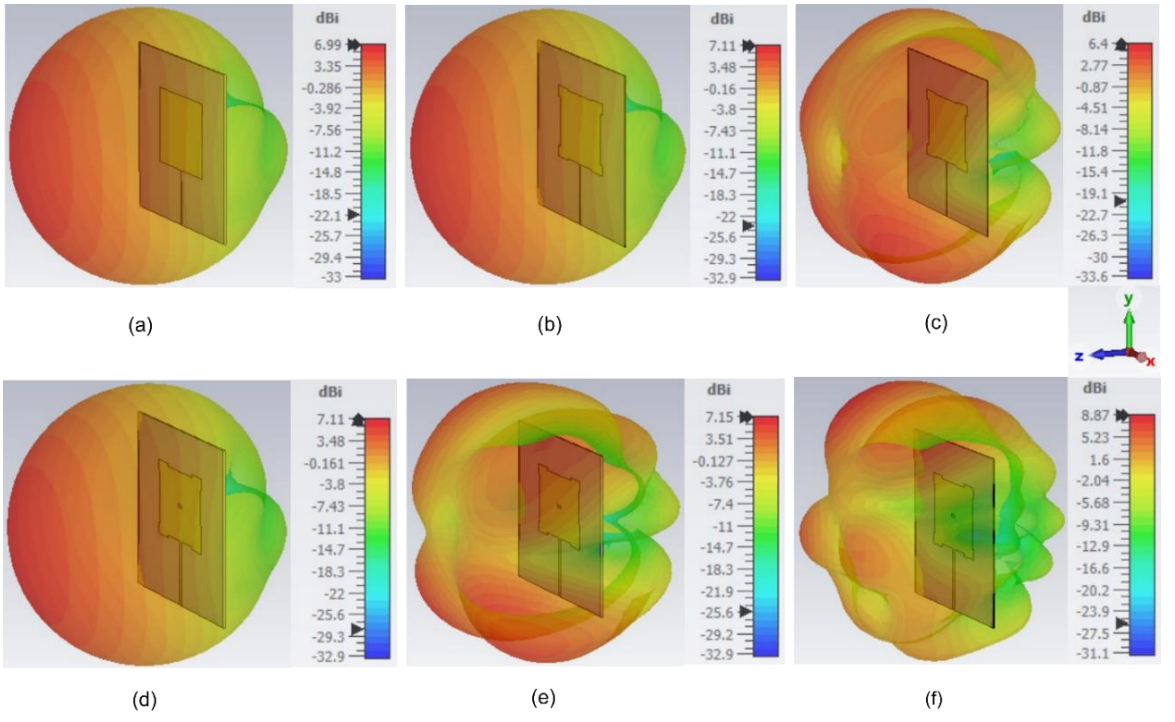

Fig. 10: 3 D far-field radiation patterns of the rectangular microstrip patch antenna at 0.7 GHz (a), the first iteration of the Minkowski fractal microstrip patch antenna at 0.7 GHz (b) and 1.8 GHz (c), and the hybrid Minkowski and Sierpinski carpet fractal microstrip patch antenna at 0.7 GHz (d), 1.8 GHz (e), and 2.6 GHz (f).

values of the simulated electric and magnetic field strengths at a frequency of 0.70 GHz. Similarly, the electric and magnetic fields in the far-field region of the microstrip antennas are normalized by the maximum values of the measured electric and magnetic field strengths at a frequency of 0.70 GHz.

In Fig. 10, the following parameters represent the antenna gains: the rectangular microstrip patch antenna at 0.70 GHz (6.99 dBi), the first iteration of the Minkowski fractal microstrip patch antenna at 0.70 GHz (7.11 dBi) and 1.80 GHz (6.4 dBi), and the hybrid Minkowski and Sierpinski carpet fractal microstrip patch antenna at 0.70 GHz (7.11 dBi), 1.80 GHz (7.15 dBi), and 2.60 GHz (8.87 dBi).

In Table 2, the proposed work is compared with previous research. The table includes fractal types, feedline types, algorithms, flexible designs at desired frequencies, and resonance and transformation frequencies focused on comparing research works. The proposed work is the most flexible design compared to other research works.

4. Discussion

Table 1 is used to configure the shapes of microstrip patch antennas−the rectangular microstrip patch antenna, the first iteration of the Minkowski fractal microstrip patch antenna, and the hybrid Minkowski and Sierpinski carpet fractal microstrip patch antenna−at the desired operating frequencies using GA. The dimensions of the microstrip patch antennas and feedlines are related to achieve matching purposes. The generated dimensions are subject to limited range constraints to prevent geometric overlap and are analyzed by crossover and mutation operations in GA. Fractal antenna designs typically use dimensions based on self-similar geometric shapes. However, implementing this in the fabrication process can be challenging due to the tiny printed circuit lines and overlapping configurations. The hybrid configurations, such as the hybrid Minkowski and Sierpinski carpet fractal microstrip patch antenna, can be an option to reduce tiny printed circuit lines and overlapping configurations. Through multiple generations of evolution, GA can converge towards the best geometric shape to achieve the desired operating frequencies of 0.70, 1.80, and 2.60 GHz. This method is especially beneficial in antenna design and electromagnetic structures, where achieving the desired operating frequencies is essential for optimal performance.

The running time of the GA process was significantly extended due to the requirement of modeling and simulating each antenna structure using CST, followed by the necessity to transfer the detailed simulation results back into the GA environment within MATLAB. Throughout this extensive procedure, the MATLAB programming codes designed for the GA meticulously manage and oversee each stage of the process, ensuring that the iterative evaluations and optimizations continue until all predetermined GA termination criteria are fully satisfied.

The microstrip patch antennas were constructed with two conductive layers of annealed copper laminated on both faces of the FR4 substrate dielectric layer (Fig. 6). It is well-known that the relative permittivity or dielectric constant of FR4 can vary from 3.8 to 4.8 (Farads per meter) F/m depending on the

Table 2: Comparison between previous research works and the proposed work.

Reference	Fractal types	Feedline types	Algorithms	Flexible designs at desired frequencies	Resonance and transformation frequencies
Abd Kadir *et al.*[7]	Sierpinski carpet	No details	IFS	Depend on the scale factor	Difficulty in maintaining control at the desired operating frequencies
Ali *et al.*[8]	Minkowski	No details	IFS	Depend on the scale factor	Difficulty in maintaining control at the desired operating frequencies
Sagne *et al.*[13]	Sierpinski carpet	Microstrip feed	IFS	Depend on the scale factor	Difficulty in maintaining control at the desired operating frequencies
Namdeo *et al.*[14]	Sierpinski carpet hybrid	Microstrip feed	IFS	Depend on the scale factor	Difficulty in maintaining control at the desired operating frequencies
Kaka *et al.*[20]	Minkowski and Sierpinski carpet	Microstrip feed	IFS	Depend on the scale factor	Difficulty in maintaining control at the desired operating frequencies
Kunwar *et al.*[21]	hybrid Minkowski and Sierpinski carpet	Coaxial feed	Manually adjusting dimensional scale using commercial software	Depend on adjustments to the dimensional scale	Difficulty in maintaining control at the desired operating frequencies
This work	customized hybrid Minkowski and Sierpinski carpet	Microstrip feed	GA	Flexible design	Flexible to maintain control at the desired operating frequencies

operating frequencies. In simulation results, however, the FR4 relative permittivity is set to a constant value of 4.3 F/m at the desired operating frequencies. It is important to note that the current distributions are strong around the sharp edges of the microstrip patch antennas, as shown in Fig. 7. However, the corners are rounded during fabrication. As a result, this can lead to different simulation and measurement results due to the variation of the dielectric constant of FR4 substrate with the operating frequencies and a different surface current on the antenna structure than the simulated ones. From Fig. 8, $S11(f_n)$ parameters show impedance matching between antenna and feedline impedances at resonance and transformation frequencies. It has also been observed that the fractional matching bandwidths of the microstrip patch antennas are considered. For the rectangular microstrip patch antenna in Fig. 8(a), the true errors of the $S11$ parameter and bandwidth between simulation and measurement results are 2.67 dB and 3.5 MHz, respectively. These discrepancies occur at the resonance frequency of 0.70 GHz for the simulation result and 0.71 GHz for the measurement result. For the first iteration of the Minkowski fractal microstrip patch antenna in Fig. 8(b), the true errors of the $S11$ parameter and bandwidth between simulation and measurement results are 1.13 dB and 4.60 MHz, respectively. These discrepancies occur at the resonance frequency of 0.70 GHz for the simulation and 0.71 GHz for the measurement result. Also, the true errors of the $S11$ parameter and bandwidth between simulation and measurement results are 8.35 dB and 1.60, respectively. The transformation frequency for the simulation result is 1.80 GHz, while for the measurement result, it is 1.82 GHz. For the hybrid Minkowski and Sierpinski carpet fractal microstrip patch antenna in Fig. 8(c), the true errors of the $S11$ parameter and bandwidth between simulation and measurement results are 2.14 dB and 3.60 MHz, respectively. These discrepancies occur at the resonance frequency of 0.70 GHz for the simulation result and 0.71 GHz for the measurement result. Also, the true errors of the $S11$ parameter and bandwidth between simulation and measurement results are 3.67 dB and 1.00 MHz, respectively. These discrepancies occur at the transformation frequency of 1.80 GHz for the simulation result and 1.82 GHz for the measurement result. Finally, the true errors of the $S11$ parameter and bandwidth between simulation and measurement results are 4.32 dB and 3.20 MHz, respectively. The transformation frequency for the simulation result is 2.60 GHz, while for the measurement result, it is 2.65 GHz. It is observed from the results above that when the number of iterations increases, the bandwidths of the microstrip patch antennas also increase, as shown in Figs. 8(b) and (c). However, there are some spurious frequencies. This is because gouging slots on the patch can create arbitrary shapes of the microstrip patch antenna. The desired operating frequencies are shifted from simulation results when compared with experiment results, especially higher frequencies, as shown in Figs. 8(b) and (c). This could be due

to the inconstant permittivity of the FR4 substrate at higher frequencies.

The far-field patterns are similar in both main lobe directions and angular widths at the same operating frequency, as demonstrated in Fig. 9. However, during the experiment, the electromagnetic radiation patterns were not smooth due to the effect of printed circuit etching. Additionally, there are minor deviations between the electric and magnetic patterns observed between the simulation and experimental results due to slight differences in frequencies. Furthermore, the radiation patterns were found to be altered with each fractal transformation of the microstrip geometry, both in the simulation and experimental results. The difference in results can be explained by the manufacturing tolerances related to the fractal design, which caused the edges to be less sharp than anticipated in the simulations. This caused the surface current on the antenna to differ from the simulated values, resulting in a change in gain. The antenna gains, as shown in Fig. 10, are not too high. It is widely understood that antenna efficiency is impacted by three types of losses: reflection loss, conductor loss, and dielectric loss. The reflection loss can be minimized using GA to align the impedances between an antenna and a feedline. However, the losses due to the conductor and dielectric are influenced by the materials selected for the antenna design.

In Table 2, two previous research papers are based on the hybrid Minkowski and Sierpinski carpet type. This combined antenna configuration design helps avoid geometric overlap to create a fractal antenna. Only one previous research paper has proposed using the coaxial feed instead of the microstrip feed. Using the microstrip feed can simplify impedance matching and integration into circuits. Traditional design of fractal antennas utilizes IFS with adjusting dimensional scales using commercial software, which can complicate maintaining control at the desired operating frequencies. This arises from challenges in determining the precise ratios of the dimension scale factors for every intended operating frequency. On the other hand, using artificial intelligence (AI) such as GA can generate dimensional scales flexibly with constraints to control desired antenna parameters. As a result, maintaining control over dimensional scales is possible for every desired operating frequency as long as the geometric overlap does not happen in real-world structures. GA can be used to design complex antenna configurations, such as hybrid fractal antennas. While GA is highly efficient in managing complex designs, it may require a significant amount of time to process fractal antenna structures with intricate geometries.[29]

A microstrip patch antenna designed for high-gain applications utilizing one-dimensional electromagnetic band gap structures− stacking of the substrate layers above the microstrip patch antenna−has been reported.[30] This research paper investigates the precise determination of band gaps through the transfer matrix method. After this analysis, an innovative design is presented to improve the antenna's directivity. The use of integrated antenna systems with payloads has been introduced.[31] This method allows for a notable enhancement in power generation by integrating the antenna system. For future work, it is possible to use techniques of one-dimensional electromagnetic band gap structures to increase the gain of fractal microstrip patch antennas, and using integrated antenna systems presents an opportunity to improve lower power consumption in wireless multifrequency applications.

5. Conclusion

In the field of geometric design, it has been observed that the use of GA optimization can successfully design rectangular microstrip patch antennas, Minkowski fractal microstrip patch antennas, and hybrid Minkowski and Sierpinski carpet fractal microstrip patch antennas at the desired operating frequencies. When designing these fractal microstrip patch antennas, it is important to consider the desired resonance and transformation frequencies and adjust the cutting slot sizes accordingly. The antenna structures can be constructed in parts of the cutting slots that do not intersect due to GA constraints. GA optimization can be employed to achieve the desired operating frequencies of 0.7, 1.8, and 2.6 GHz by optimizing the shapes and dimensions of the antenna. It should be noted that the desired operating frequencies in this research paper are just examples and can be adjusted based on the specific design requirements for future work. Furthermore, due to the high coupling effects between cutting slots and dimensional constraints imposed by higher iterations, which can deteriorate antenna matching, optimizing the feedlines using GA can be a viable solution. This can be true in practice. The trend of the experimental results is consistent with the simulation results. Some errors between simulation and experiment results will be controlled very close to each other.

Acknowledgements

The research project and publication of this research paper were funded by the Faculty of Engineering, Srinakharinwirot University, Thailand.

Conflict of Interest

There is no conflict of interest.

Supporting Information

Not applicable.

References

[1] M. Kanthi, R. Dilli, Wireless Sensor Networks: Network Life Time Enhancement using an Improved Grey Wolf Optimization Algorithm, *Engineered Science*, 2022, **19**, 186-197, doi: 10.30919/es8d717.

[2] J. Singh, Energy efficient data aggregation and density-based spatial clustering of applications with noise for activity monitoring in wireless sensor networks, *Engineered Science*, 2022, **19**, 144-153, doi: 10.30919/es8d694.

[3] N. Guler, M. Salamah, Adaptive resource allocation scheme for cooperative transmission in hybrid simultaneous wireless information and power transfer for wireless powered sensor networks, *Engineered Science*, 2023, **25**, 932, doi: 10.30919/es932.
[4] P. Kumar, T. Ali, M. Pai, Highly isolated ultrawideband multiple input and multiple output antenna for wireless applications, *Engineered Science*, 2022, **17**, 83-90, doi: 10.30919/es8d570.
[5] S. K. Singh, T. Sharan, A. K. Singh, Enhancing the axial ratio bandwidth of circularly polarized open ground slot coplanar waveguide-fed antenna for multiband wireless communications, *Engineered Science*, 2022, **17**, 274-284, doi: 10.30919/es8d557.
[6] K. Thenkumari, K. S. Sankaran, J. M. Mathana, Design and implementation of frequency reconfigurable antenna for Wi-Fi applications, *Engineered Science*, 2023, **23**, 876, doi: 10.30919/es8d876.
[7] M. F. Abd Kadir, A. S. Ja'afar, M. Z. A. Abd Aziz, Sierpinski carpet fractal antenna, Asia-Pacific Conference on Applied Electromagnetics Proceedings, 2007, 1-4, doi: 10.1109/APACE.2007.4603961.
[8] J. K. Ali, A new reduced size multiband patch antenna structure based on minkowski pre-fractal geometry, *Journal of Engineering and Applied Sciences*, 2007, **2**, 1120-1124.
[9] C. Gibson, J. A. de Lemos, E. M. Antman, Fractal geometry and design of modern structures, *E3S Web of Conferences*, 2021, **281**, 1-8, doi: 10.1051/e3sconf/202128102018.
[10] V. M. Onufrienko, The frequency independence of fraction antennas, International Conference on Antenna Theory and Techniques, 2013, 332-334, doi: 10.1109/ICATT.2013.6650768.
[11] Y. Nakanishi, Y. Namiki, K. Hongo, J. Urata, I. Mizuuchi, M. Inaba, Design of the musculoskeletal trunk and realization of powerful motions using spines, IEEE-RAS International Conference on Humanoid Robotics, 2007, 96-101, doi: 10.1109/ICHR.2007.4813854.
[12] W. Chen, G. Wang, Small size edge-fed Sierpinski carpet microstrip patch antennas, *Electromagnetics Research C*, 2008, **3**, 195-202, doi: 10.2528/PIERC08050302.
[13] D. S. Sagne, R. S. Batra, P. L. Zade, Design of modified geometry Sierpinski carpet fractal antenna array for wireless communication, 3rd IEEE International Advance Computing Conference, 2013, 435-439, doi: 10.1109/IADCC.2013.6514265.
[14] P. Namdeo, N. Agrawal, P. Yadav, R. Vishwakarma, G. Chaitanya, Design and analysis of Sierpinski carpet fractal antenna, *International Journal of Innovative Research in Electrical, Electronics, Instrumentation and Control Engineering*, 2015, **3**, 47-49, doi: 10.17148/IJIREEICE.2015.3514.
[15] J. W. Jayasinghe, Application of genetic algorithm for binary optimization of microstrip antennas: A review, *AIMS Electronics and Electrical Engineering*, 2021, **5**, 315-333, doi: 10.3934/electreng.2021016.
[16] M. Lamsalli, A. E. Hamichi, M. Boussouis, N. A. Touhami, T. Elhamadi, Genetic algorithm optimization for microstrip patch antenna miniaturization, *Progress in Electromagnetics Research Letters*, 2016, **60**, 113-120, doi: 10.2528/PIERL16041907.
[17] M. K. Dhakshinamoorthi, S. Gokulakkrizhna, K. M. Denesh, M. Subha, V. Mekaladevi, Rectangular microstrip patch antenna miniaturization using improvised genetic algorithm, Proceedings of the Fourth International Conference on Trends in Electronics and Informatics, 2020, 894-898, doi: 10.1109/ICOEI48184.2020.9142912.
[18] S. Koziel, O. Saraereh, J. W. Jayasinghe, D. Uduwawala, Local optimization of a sierpinski carpet fractal antenna, IEEE International Conference on Industrial and Information Systems, 2017, 15-16, doi: 10.1109/ICIINFS.2017.8300415.
[19] D. Uduwawala, J. Jayasinghe, N. Narampanawe, Genetically designed high gain sierpinski carpet fractal antenna, IEEE International Conference on Industrial and Information Systems, 2019, 18-20, doi: 10.1109/ICIIS47346.2019.9063309.
[20] A. Kaka, M. Toycan, V. Bashiry, H. Ademgil, S. D. Walker, A fractal geometry, multi-band, miniaturized monopole antenna design for UWB wireless applications, IEEE-APS Topical Conference on Antennas and Propagation in Wireless Communications, Turin, Italy, 2011, 584-587, doi: 10.1109/APWC.2011.6046785.
[21] A. Kunwar, A. K. Gautam, B. K. Kanaujia, Triple-band antenna combining Minkowski and modified Sierpinski fractal geometry, IEEE Applied Electromagnetics Conference (AEMC), Guwahati, India, 2015, 1-2, doi: 10.1016/j.measurement.2021.109766.
[22] C. A. Balanis, Antenna theory: analysis and design, New Jersey: John Wiley & Sons, 2022, 816-825, ISBN: 978-1-118-64206-1.
[23] N. Abdullah, A. M. Shire, M. A. Ali, E. Mohd, Design and analysis of minkowski fractal antenna, *ARPN Journal of Engineering and Applied Sciences*, 2015, **10**, 8736-8739.
[24] M. S. Maharana, G. P. Mishra, B. B. Mangaraj, Design and simulation of a sierpinski carpet fractal antenna for 5G commercial applications, IEEE WiSPNET Conference, 2017, 1718-1721, doi: 10.1109/WiSPNET.2017.8300056.
[25] R. L. Haupt, S. E. Haupt, Practical genetic algorithms, John Wiley & Sons, 2004, ISBN:9780471455653.
[26] B. R. Behera, Sierpinski bow-tie antenna with genetic algorithm, *Engineering Science and Technology, an International Journal*, 2017, **20**, 775-782, doi: 10.1016/j.jestch.2016.10.017.
[27] S. M. Villada, E. Reyes-Vera, M. Arias-Correa, AnIMAGE: A MATLAB-based tool for generating microstrip antennas with complex shapes, *SoftwareX*, 2023, **23**, 101502, doi: 10.1016/j.softx.2023.101502.
[28] A. Baldominos, S. Mercader-Pellicer, G. Goussetis, A. Mengali, N. J. Fonseca, Heras: a modular matlab tool using physical optics for the analysis of reflector antennas, *Sensors*, 2023, **23**, 1425, doi: 10.3390/s23031425.
[29] A. Douklias, A. Dadoukis, S. Athanasiadis, A. Amditis, A field communication system for volunteer urban search and rescue teams combining 802.11 ax and LoRaWAN, *Applied Sciences*, 2023, **13**, 6118, doi: 10.3390/app13106118.

[30] S. Said, O. El melhaoui, Y. Guetbach, E. Baghaz, A. Faize, Design of a patch antenna for high-gain applications using one-dimensional electromagnetic band gap structures, *Engineered Science*, 2024, **27**, 1040, doi: 10.30919/es1040.
[31] G. G. A. Ibrayev, N. Meirambekuly, B. Karibayev, T. Namazbayev, S. Orynbassar, A. Sukhenko, A. Temirbayev, A. Zhauyt, Reducing energy consumption in cubeSat missions: the integrated antenna approach, *Engineered Science*, 2025, **33**, 1315, doi: 10.30919/es1315.